https://doi.org/10.5194/angeo-2023-34
Preprint. Discussion started: 30 November 2023

Annales Geophysicae Discussions

The Role of Gravity Waves in the Mesosphere Inversion Layers (MILs) over low-latitude (3-15^0 N) Using SABER Satellite Observations

Chalachew Lingerew[1*], U. Jaya Prakash Raju[1]

[1] Department of Physics, Washera Geospace, and Radar Science Laboratory, Bahir Dar, Ethiopia, Bahir Dar University

Correspondence to: Chalachew Lingerew (chalachewlingerew@gmail.com)

Abstract

The Mesosphere transitional region over low latitude is a distinct and highly turbulent zone of the atmosphere. A transition mesosphere region is connected with dynamic processes, particularly gravity waves, as a causative of an inversion phenomenon. Mesospheric inversions have been the subject of numerous investigations, but their formation mechanisms are still poorly understood. In this article, an attempt has been made to investigate the upper and lower inversion phenomena and their causative mechanisms using long-term SABER observations in the height range of 60-100 km during the period of 2005-2020 over a low-latitude region (3-15^0 N). The results indicate that the frequency of occurrence rate for the upper inversion is below 40%, whereas for the lower inversion, it is below 20%, indicating that the upper inversion is dominant over the lower inversion. The upper inversion exists in the height range of 78-91 km with an inversion amplitude of ~20-80 k and a thickness of ~3-12 km, whereas the lower inversion is confined in the height range of 70-80 km with an inversion amplitude of ~10-60 k and a thickness of ~4-10 km. The gravity wave indicator potential energy depicts high energy (below 100 J/kg) in the upper mesosphere region (90 and 85 km) compared to the lower mesosphere region (75 and 70 km) with less than 50 J/kg. The stability criteria from Brunt-Vaisala frequency (N^2) indicate instability in the upper mesosphere region (90 and 85 km) with very low values relative to the lower mesosphere region (75 and 70 km), which supports the higher frequency of upper inversion compared to lower inversion. This result leads us to the conclusion that a high amount of gravity wave potential energy is a consequence of the high instability in the upper inversion relative to the lower inversion.

Keywords. Mesosphere, Upper and Lower Inversions, Perturbed temperature, Causative gravity waves, Potential Energy, Brunt-Vaisala frequency, Instability.

https://doi.org/10.5194/angeo-2023-34
Preprint. Discussion started: 30 November 2023

Annales Geophysicae Discussions Open Access EGU

Introduction

The mesosphere dynamic regions act as a transition zone to the lower and upper atmospheric wave processes (tidal waves, planetary waves, and gravity waves). It is a well-known fact that atmospheric waves, especially gravity waves (GWs) generated from the lower atmosphere, propagate into the middle and upper atmospheres, break in the mesosphere region during propagation, and dissipate their energy and momentum into the background atmosphere, influencing the dynamics of the mesosphere thermal structure, global atmospheric circulation, variability, and even the MIL phenomenon (Lindzen, 1981; Holton, 1983). The Mesospheric Inversion Layer (MIL) is a feature of the mesosphere region in the temperature profile. The MIL is a symptom (sign) of wave saturation in the mesospher because the temperature inversion occurs at altitudes when the lapse rate is less than half of the dry adiabatic lapse rate (Sica et al., 2007). Temperature inversions have been omnipresent features in the mesosphere regions for decades, and they have been comprehensively studied in the past by using all sorts of available techniques (e.g., lidar, radar, rocket sonde, and satellite) over different geographic locations.

Because of gravity waves (GWs) momentum and energy deposition, it is thought to be the principal mechanism driving large-scale circulation and coupling of distinct atmospheric layers, as well as inversion phenomena (Fritts and Alexander, 2003; Lindzen, 1981; Smith, 2012). In addition, the gravity wave-breaking influence on mesosphere dynamics is an attempt to demonstrate the emergence of the inversion phenomenon over mid and high latitudes (Gan et al., 2012; Walterscheid and Hickey, 2009; Collins et al., 2011; Szewczyk et al., 2013). Observational and modeling approaches have been used to investigate GWs as the causative of inversions (Fritts, 2018; Collins et al., 2014; Sridharan et al., 2008; Ramesh and Sridharan, 2012; Ramesh et al., 2013, 2014, 2017). The effect of gravity waves in the mesosphere inversion based on temperature variability is studied particularly over the mid- and high-latitudes (Singh and Pallamraju, 2018; Fritts et al., 2018). As a result, the inversion phenomenon has been the topic of numerous studies in mesosphere dynamics, yet the mechanisms of development have been poorly understood.

Regarding low latitudes, there are very less number of studies on the altitudinal, latitudinal, and longitudinal variability of the mesosphere inversion phenomenon associated with gravity wave activity. This provides motivation to investigate the mesosphere inversion phenomenon and its association with gravity wave activity, along with stability criteria using Brunt-Vaisala frequency (N^2) over the low latitudinal band (3-15^0 N) using long-term SABER observations during 2005-

https://doi.org/10.5194/angeo-2023-34
Preprint. Discussion started: 30 November 2023

2020. This is organized as follows: The data and method of extracting the mesosphere inversion phenomenon are presented in Section 2, and their results are described in Section 3. Finally, Section 4 presents the conclusions.

2. Observation and Data analysis

2.1 SABER Observation

The TIMED/SABER satellite was launched on December 7, 2001, to set on an elliptical orbit at an altitude of about 625 km with an inclination of 74^0 from the equator. The SABER instrument makes 15 orbits; each orbit takes 97 minutes (1.6 h) and provides about 1400 profiles; each profile takes 58 seconds. This TIMED/SABER satellite provides temperature profiles with good spatial and temporal resolution to investigate mesosphere dynamics and their atmospheric wave processes (Nath, O., and Sridharan, S., 2014; Gan et al., 2012; Bizuneh et al., 2022; Lingerew et al., 2023). In the present study, the SABER vertical temperature profiles in the region of 60-100 km altitude during the period January 2005-December 2020 over the low latitudes (3-15^0 N) are used to investigate the dynamics of the lower and upper mesosphere inversion phenomena and their causatives, as shown in Figure 1. The monthly mean temperature of the mesosphere region (60-100 km) shows a maximum temperature of 200-240 K in the height range of 60-70 km, with the minimum temperature declining to around 160-180 K in the height range of about 95-100 km throughout the period.

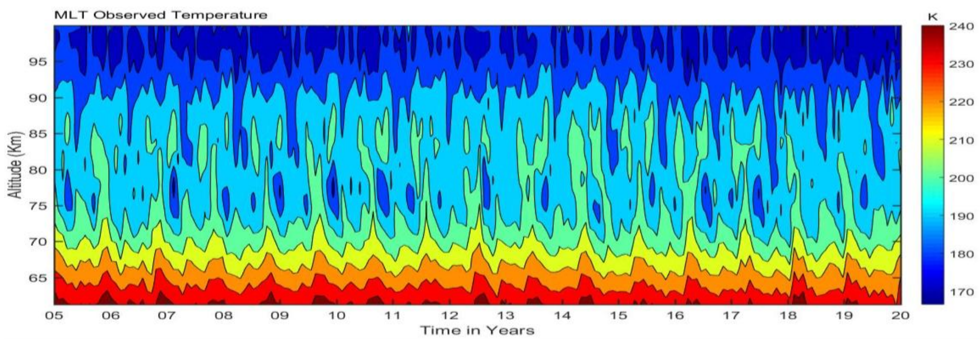

Figure 1. The monthly mean mesosphere temperature variability in the height range of 60-100 km during December 2005-January 2020 over the low latitude.

2.2 Analysis technique

Mesosphere inversions of temperature are identified based on their characteristics-thickness, and amplitude-corresponding to an altitude and temperature difference between the top and bottom

https://doi.org/10.5194/angeo-2023-34
Preprint. Discussion started: 30 November 2023

Annales Geophysicae Discussions

levels (Leblanc and Hauchecorne, 1997; Fechine et al., 2008). In this investigation, the upper and lower mesosphere inversions are identified using the following criteria: (1) The bottom level of the lower and upper inversions is above 65 and 80 km, and its top level of inversion is below 78 and 92 km, respectively; (2) the amplitude is considered larger than 5 K; and (3) the thickness is greater than or equal to 2 km following the procedure. Inversions that satisfy the above-mentioned criteria are considered significant. Based on this sequence of temperature inversion, diagnostic techniques were applied to the daily SABER observation data during the period 2005-2020 over low latitudes. This inversion of the mesosphere temperatures is related to their instabilities.

Brunt-Vaisala frequency is used to characterize atmospheric stability.

$$N^2(z) = \frac{g(z)}{T_0(z)}\left(\frac{\partial T_0(z)}{\partial z} + \Gamma_d\right) \quad (1)$$

Where g is the acceleration due to gravity, N is the Vaisala frequency, T_0 is the background temperature, estimated based on the third-order polynomial fitting, $\Gamma_d = {}^{g}/{c_p}$ is the adiabatic lapse rate, and $c_p = 1004\, J\, K^{-1}\, kg^{-1}$ is the specific heat capacity of the atmosphere at constant pressure. When Vaisala frequency N^2, is statically positive, the atmosphere is stable. While the frequency N^2, is negative, the atmosphere is unstable, in which the atmospheric lapse rate, $\Gamma = -\frac{\partial T}{\partial z}$ is larger than the adiabatic lapse rate, ${}^{g}/{c_p} \approx 9.5\, K\, km^{-1}$, the atmosphere is unstable.

The third-order polynomial fit of the least squares has been applied to estimate the background temperature (T_0) from the observed temperature (T) following the procedure adopted by Ramesh and Sridharan (2012). In order to identify the impacts of gravity waves on atmospheric temperature variability, the perturbed temperature (T_p) is estimated by subtracting the background from the observed temperature data (T).

$$T_p = T - T_0 \quad (2)$$

After the perturbed temperature is calculated, a 1-hour interval of the cutoff frequency of the low-pass band filter is used to remove the planetary and tidal wave contributions in order to extract short-period gravity waves. This filtered perturbed temperature, Tp, is used to estimate the potential energy (E_P) (John and Kumar, 2012) to understand the atmospheric gravity waves.

$$E_p(z) = \frac{1}{2}\left(\frac{g(z)}{N(z)}\right)^2 \left(\frac{T_p(z)}{T_0(z)}\right)^2 \quad (3)$$

https://doi.org/10.5194/angeo-2023-34
Preprint. Discussion started: 30 November 2023

These fluctuations are extracted and subjected to further analysis to estimate the potential energy of the waves as a function of altitude, z, which quantifies the wave activity of the region under study.

3. Results and discussion

3.1 Identification and Characteristics of the Lower and Upper MLT Inversion

The daily SABER temperature profiles of upper and lower mesosphere during the period of 2005–2020 over low latitudes (3-15^0 N) are depicted in the form of contours in Figure 2(a and c). The corresponding contours drawn in the lower panels of Figure 2(b and d) are the daily inversion mesosphere temperature profiles. The upper panel on the left side of Figure 2(a) represents the daily upper mesosphere observed temperature variability, which is depicted in the range ~(180-205 K) at the height around ~80-90 Km, and the right upper panel of Figure 2(c) represents the lower mesosphere temperature variability at the range around ~(180-220 K) at the height around ~70-80 Km.

Whereas, the left side of the lower horizontal panel of Figure 2(b) represents the upper inversion layer of temperature around ~(180-220 K) at the upper mesosphere region around ~(80-90 Km) is minimum compared to the right side of the lower panel of Figure 2(d) of the lower inversion temperature in the range ~(180-225 K) at the lower mesosphere region in the height around ~(70-80 Km), which refers to the temperature gradient from negative to positive observed due to external or internal drivers.

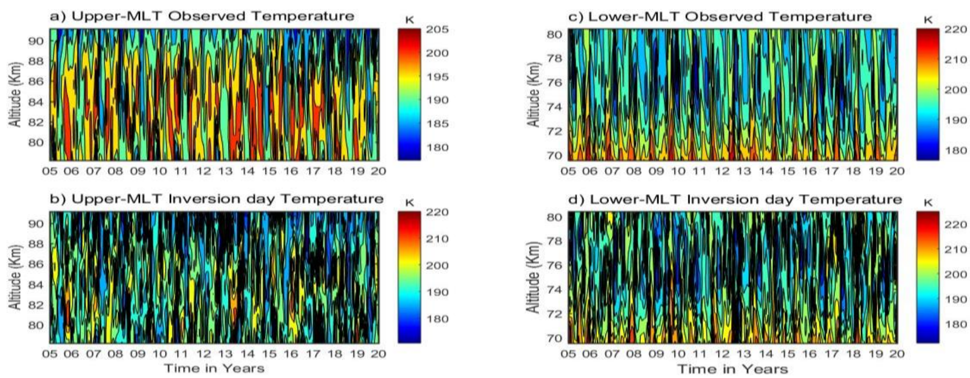

Figure 2. The upper and lower mesosphere observed temperatures in the first horizontal panel at (a and c) with their inversions in the second horizontal panel at (b and d).

https://doi.org/10.5194/angeo-2023-34
Preprint. Discussion started: 30 November 2023

Annales Geophysicae Discussions
Open Access

The observed temperatures in the first horizontal panel, as indicated in Figure 2(a and c), have shown minimum values when compared to the SABER inversion temperatures in the second horizontal panel (Figure 2(b and d)). Our findings are similar to previous reports by Siva Kumar et al. (2001), which show that the base of the lower mesospheric inversion layer (MILs) lies in the range of 73-79 km, with a peak of about 76 km. Similarly, Szewczyk et al. (2013) reported double mesospheric inversions at 71-73 km altitude with minimal amplitude compared to upper inversions at altitudes of 86-89 km.

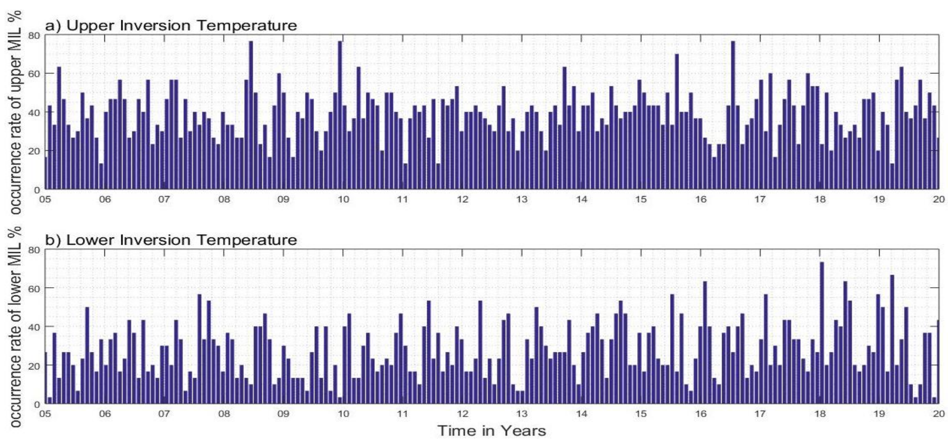

Figure 3. The frequency occurrence rate (percentage) of the (a) upper and (b) lower inversion temperatures during 2005-2020 over low latitudes.

Further, the frequency occurrence (%) of mesospheric inversion layers (MILs) is investigated for the period 2005-2020, and the results are displayed in the form of a histogram in Figure 3(a) for the upper MIL and in Figure 3(b) for the lower MIL. The mean frequency occurrence rate of the upper inversion is approximately below 40%, and the maximum rate of the upper inversion lies between 60% and 78%, particularly in the years 2008, 2010, and mid-2016. While the mean frequency occurrence rate of the lower inversion is below 20%, In general, the occurrence rate of the upper inversion is relatively high compared with the lower inversion, which could be related to the atmospheric wave activities, particularly gravity wave activity, which is high in the upper mesosphere compared to the lower mesosphere atmospheric region (Hauchecorne et al., 1987; France et al., 2015).

Generally, the mesospheric inversion layer phenomenon is characterized by identifying inversion base height, inversion amplitude, and inversion thickness. The temperature and height differences between the inversion layers at the bottom and top are defined as the amplitude and thickness. The

https://doi.org/10.5194/angeo-2023-34
Preprint. Discussion started: 30 November 2023

frequency of occurrence of amplitude, thickness, and base height of inversion are shown in the form of the histogram for upper and lower mesosphere in Figure 4(a-f) along with standard deviations (SD). In the left vertical column, three rows represent a histogram of (a) amplitude, (b) thickness, and (c) the base of the upper MIL phenomenon. The corresponding three rows of the right vertical column represent (d) amplitude, (e) thickness, and (f) the base of the lower MIL phenomenon.

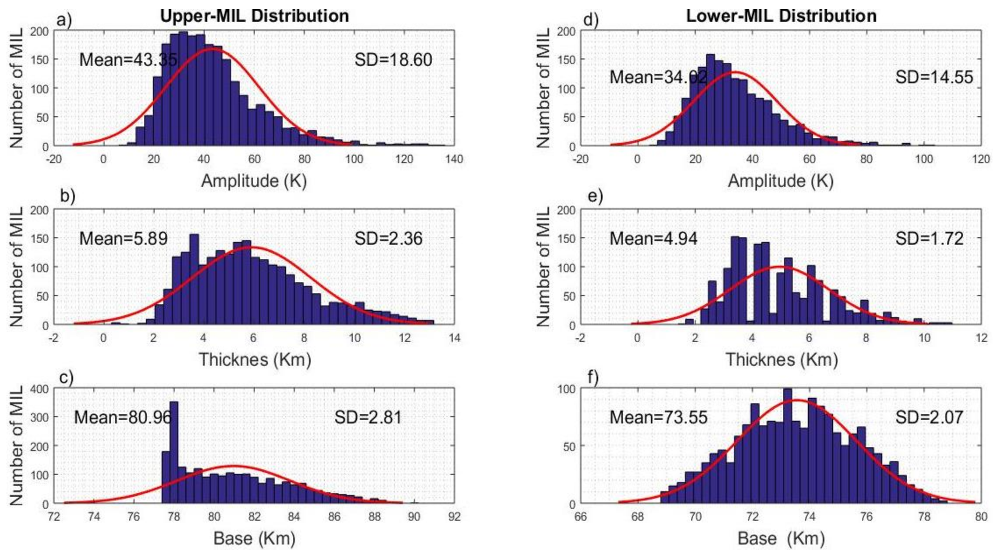

Figure 4. Histogram occurrence of mesosphere inversions. The first vertical panel represents the upper inversion distribution of (a) amplitude, (b) thickness, and (c) base, and the corresponding distribution in the second vertical panel is the lower inversion of (d) amplitude, (e) thickness, and (f) base over the low latitude during the period 2005–2020.

The upper inversion amplitude exists in the range between 20 and 80 K, with a peak value of 38 K following a Gaussian distribution with large standard deviations (SD) of 18.6 (Figure 4(a)). The thickness of the inversion layer for upper MILs has existed in the range of 3-9 K, with the most probable value of 5.5 K and a low standard deviation (SD) of 2.3 (Figure 4(b)). The base height of the upper MIL ranges from 77.5 to 90 km, with a peak value of around 78 km showing a lower standard deviation (SD) of 2.8. Whereas, the lower inversion amplitude is depicted in the range between 10 and 60 K with a peak of 25 K and standard deviations (SD) of 14.5 (Figure 4(b)). The thickness of an inversion has appeared in the range of 3-8 Km, with the most probable value of 3.8 Km and a low standard deviation (SD) of 1.72 (Figure 4(d)). The base height of the lower inversion is in the range of 69 and 78 km, with a peak value around 73 km, showing a lower standard deviation (SD) of 2.07.

https://doi.org/10.5194/angeo-2023-34
Preprint. Discussion started: 30 November 2023

Annales Geophysicae Discussions

3.2 Latitudinal Variations of Mesospheric Inversion Layers (MILs)

In this section, the spatiotemporal (latitudinal-time) variability of the MIL phenomenon is characterized based on amplitude, thickness, and base over the low latitude band (3-15^0 N) during the period of 2005-2020 using the corresponding contour plots of time vs. latitude in Figures 5(a), 5(b), and 5(c), respectively. The Upper MILs phenomenon is observed around 80-90 km, with the maximum amplitude in the range of 90-120 K over all the latitude bands (5^0-12^0 N) during 2005, 2007, mid-2011, 2013, 2015, 2016, mid-2019, and 2020. The inversion thickness depicted in the second horizontal panel, as shown in Figure 5(b), is displayed with a maximum range of ~(8-12 Km) over the entire latitudinal region (3-15^0 N). Figure 5(c) displays the relative maximum inversion base height around ~(84-88 Km) in the latitudinal range between 4 and 14^0 N during 2006, 2008, 2010, 2012, 2016, and 2018.

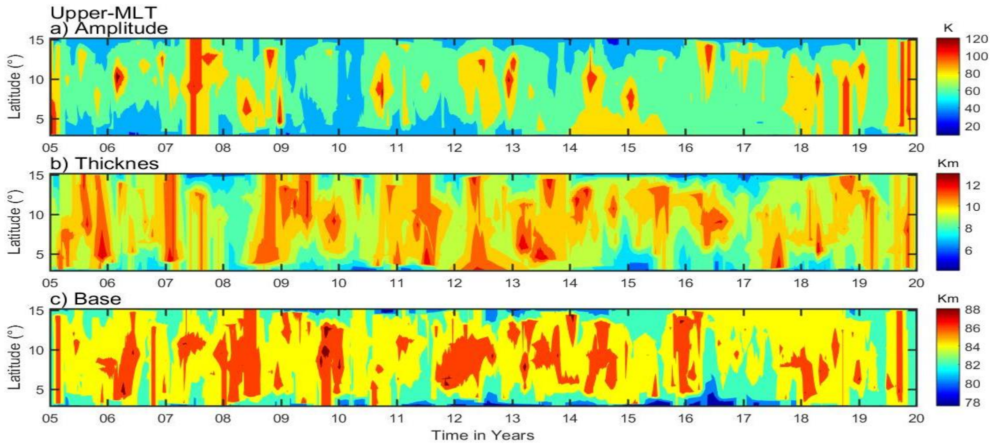

Figure 5. The daily upper inversions (~80-90 km) of (a) amplitude, (b) thickness, and (c) base height during 2005-2020 over latitudinal variation.

Similarly, the latitudinal variations of the lower inversion (MILs) phenomenon based on their characteristics amplitude, thicknesses, and base height are depicted in the form of contour plots of time vs. latitude in Figure 6(a, b, and c), respectively, over the altitudinal range around ~(70-80 km). The lower inversion amplitude is depicted in the range of ~30-60 k over all latitudinal bands except the maximum range of ~(80-100 k) during 2013, 2015, 2016, and 2019 in different latitudinal regions enclosed in the range between 5 and 14^0 N. Figure 6(b) displays the inversion thickness of 5-7 km over the entire latitude band, except for the maximum thickness of 8-10 km. The inversion of base height (76-80) is depicted in Figure 6(c) over all latitudes and periods except 2008, 2014, and mid-year 2018 with maximum base height. Figures 5 and 6, clearly show that the

https://doi.org/10.5194/angeo-2023-34
Preprint. Discussion started: 30 November 2023

high amplitude and thickness of the upper inversion in comparison with the lower inversion indicate a highly dynamical phenomenon over the upper mesosphere region.

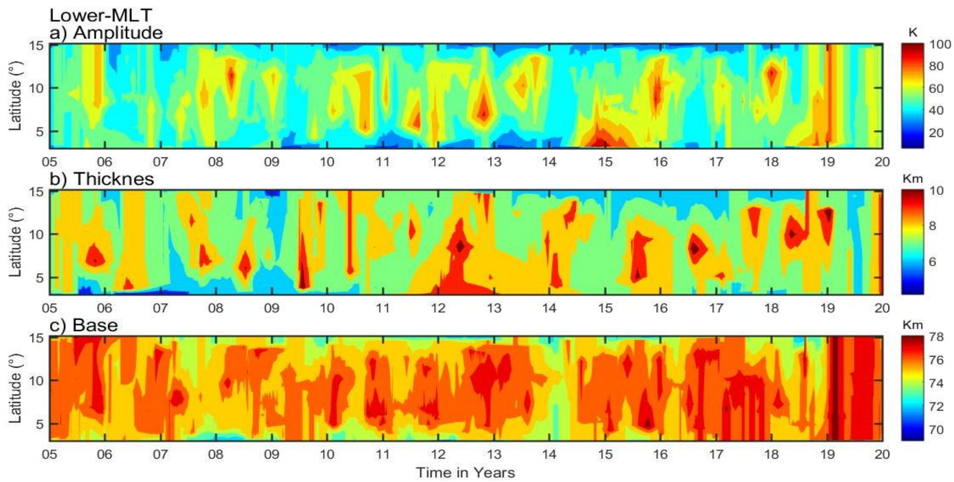

Figure 6. Same as figure 5, but for the lower mesosphere inversions (~70- 80 km).

From Figures 5 and 6, it is clearly observed that the upper inversion amplitude and thicknesses show high values in comparison with the lower inversion, indicating a highly dynamic phenomenon over the upper mesosphere region.

3.3 Separations of the Perturbed Temperature in the Mesosphere Region

Perturbed temperature profiles (T_p) at inversion days during the period of 2005-2020 in the upper and lower mesosphere regions can further be used to calculate the potential energy of gravity waves and Brunt-Vaisala frequencies (N^2). The procedure for calculating perturbation temperature (T_p) is mentioned in the methodology part.

First, the daily upper inversion profiles are identified in the upper mesosphere region during the entire observational period of 2005-2020, as displayed from the contour plot in Figure 7(a). It is noted that the inversion temperature is in the range of ~170-220 K with less detectable variability. Based on an inversion temperature profile, the background temperature (T_0) is calculated by applying a 3rd order polynomial fit, and the corresponding contour plot is drawn in Figure 7(b). This background temperature clearly displays identifiable periodic variability in the range of ~195-197 K around ~82-87 km. While the perturbed temperature profiles (T_p) are based on the difference between the observed inversion temperature (T) and the corresponding background temperature profiles (To), they display in the range of -25 to +25 K, as shown in Figure 7(c).

https://doi.org/10.5194/angeo-2023-34
Preprint. Discussion started: 30 November 2023

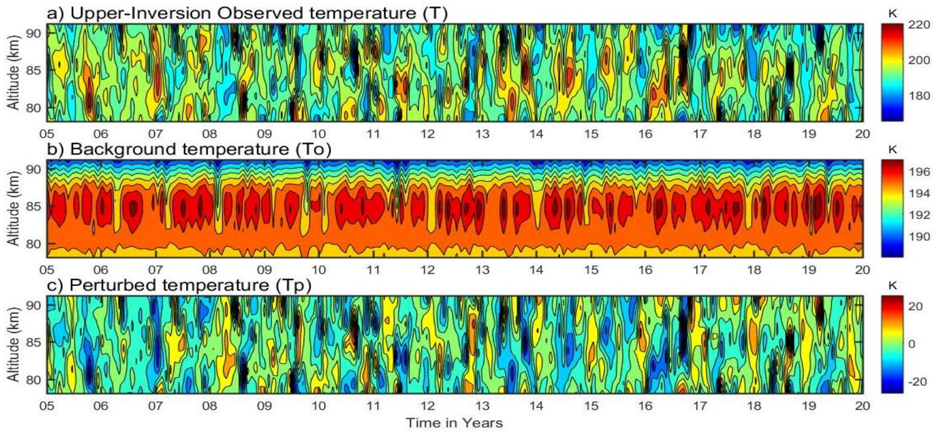

Figure 7. The upper mesosphere temperatures in the vertical panel are: (a) inversion day observed temperature; (b) background temperature; and (c) perturbed temperature in the upper mesosphere region.

A similar procedure has been applied to calculate the perturbed temperature (T_p) as well as the observed and background temperature during the period of 2005-2020 in the lower mesosphere region, and their corresponding contours are displayed in Figure 8(a-c). The observed temperature of lower inversion in Figure 8(a) depicted a range of ~170-220 K and the background temperature of lower inversion in the range of ~ 195-210 K with their maximum values of ~200-210 K over the height of ~70-72 Km as shown in Figure 8(b). Whereas the perturbed temperature in Figure 8(c) is presented in the range between -25 and 20 K. It is noted that the upper mesosphere perturbed temperature is at its maximum compared to the lower mesosphere region, which may be due to a high dynamic phenomenon.

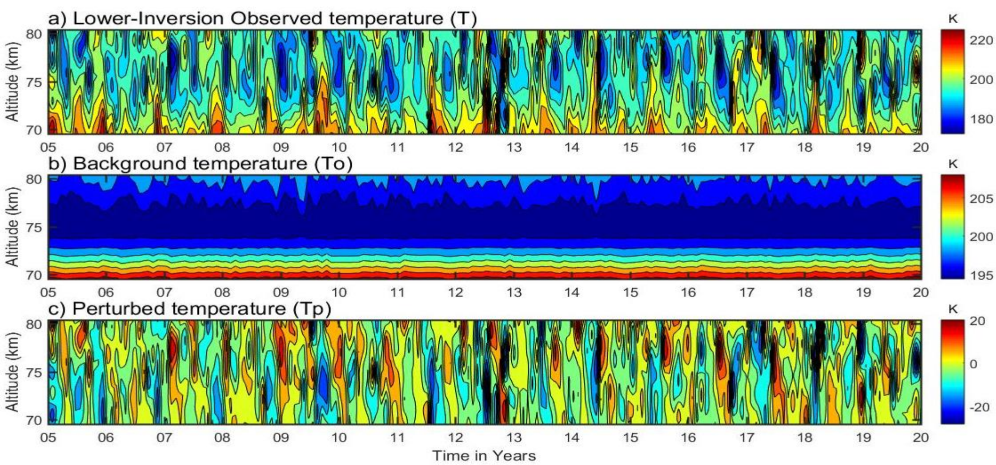

Figure 8. Same as figure 7, but for the lower mesosphere atmospheric region.

https://doi.org/10.5194/angeo-2023-34
Preprint. Discussion started: 30 November 2023

Annales Geophysicae
Discussions

3.4 Effects of Gravity Waves on Mesosphere Inversions and associated Instability

In this section, an attempt has been made to investigate the longitudinal variability of gravity waves' contribution to the mesospheric inversions (MILs) phenomenon by calculating potential energy and their instability based on Bruent-Vaisala frequency (N^2) using perturbed temperatures. A one-hour interval cut-off frequency of a low-pass band filter is applied to a perturbed temperature to remove unwanted influences on an inversion during the period 2005-2020 at selected heights of 90, 85, 75, and 70 km, as depicted in Figure 9 (a, b, c, and d), represented by a blue line plot. The reason behind using the low-pass band filter is to eliminate the influence of long-period oscillations such as tidal or planetary waves. The effects of the low-pass filter are clearly visible before and after applying the filter in Figure 9(a and b) for the upper mesosphere region at 90 and 85 km and in Figure 9(c and d) for the lower mesosphere region at 75 and 70 km. The amplitude of the perturbed temperature is reduced to the range around ~(-10 to 10 K), and the data is smoothed by eliminating higher frequencies.

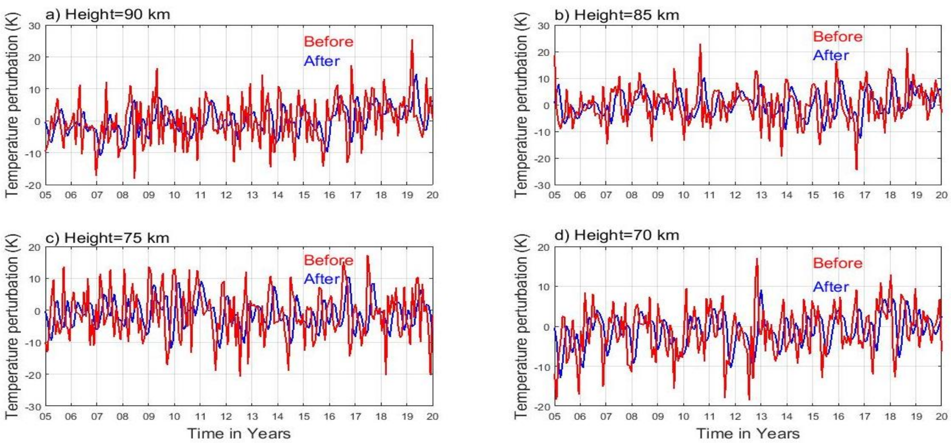

Figure 9. Perturbed temperature profiles before (red color) and after (blue color) applying the low-pass band filter for the upper (85 and 90 km) and lower (70 and 75 km) regions.

By using the time series of filtered perturbed temperature data at selected heights of 90, 85, 75, and 70 km, the potential energy (E_p) is constructed based on the formula mentioned in the methodology section, since gravity wave activity is projected by potential energy calculation by numerous authors (Tsuda et al., 2000; Wang and Geller, 2003; Liu et al., 2014; Thurairajah et al., 2014). The spatiotemporal variability of gravity wave potential energy is shown in Figure 10(a and

https://doi.org/10.5194/angeo-2023-34
Preprint. Discussion started: 30 November 2023

b) for the upper mesosphere region at (90 and 85 km) and Figure 10(c and d) for the lower mesosphere region at (75 and 70 km).

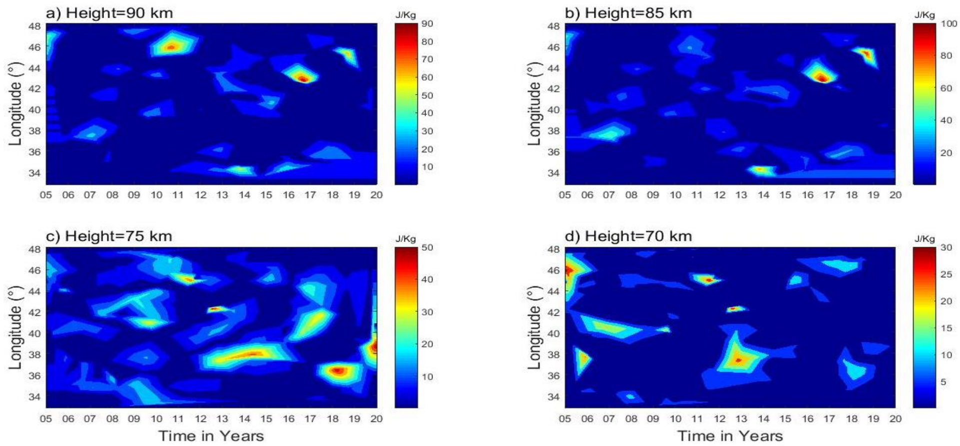

Figure 10. Gravity wave potential energy for the upper (85 and 90 km) and lower (70 and 75 km) mesosphere regions.

The maximum gravity wave potential energies in the range around ~70-90 J/kg are observed over the longitudinal regions of $45-47^0$ E, 43^0 E, and 44^0 E during 2011, 2017, and 2019 (Figure 10(a)) for upper mesosphere inversions at 90 km, whereas low potential energy around ~10-60 J/kg is presented all over the longitudinal region from $33-48^0$ E. While at 85 km shown in Figure 10(b), the maximum potential energy is around ~(70-100 J/kg) over the longitudinal (34^0, 44^0, and 46^0) regions during the period of 2014, 2016, and 2018. The low potential energy between 20 and 70 J/kg appears in all the longitude (33-48) regions. The gravity wave potential energy is presented in Figure 10 (c and d) for the lower mesosphere region at 75 and 70 km. At a height of 75 km, the maximum potential energy appeared in the range of 40-50 J/kg over the longitudinal (46^0, 42^0, 40^0, 37^0, 36^0, and 38^0) region during 2011, 2012, 2017, 2013–2015, 2018, and 2020. Similarly, Figure 10(d) depicts the gravity wave potential energy in the range of 2–30 J/kg for the lower mesosphere region at 70 km over the longitudinal region ($33-48^0$). Out of which, the maximum potential energy is found in the range between 25 and 30 J/kg in a certain longitude region and time period. The result concludes that the observation of high potential energy in the upper mesosphere region is due to the deposition of high energy and momentum at the background temperature by gravity wave breaking, which could influence the dynamics of the inversion phenomenon. The gravity

https://doi.org/10.5194/angeo-2023-34
Preprint. Discussion started: 30 November 2023

Annales Geophysicae
Discussions
Open Access

wave dynamics are multi-scale in nature; small-scale waves might contribute predominantly to instabilities, turbulence, and mixing (Liu and Meriwether, 2004; Szewczyk et al., 2013).

Hence, in this part, an attempt has been made to investigate the gravity wave contribution to the MIL phenomenon of an unstable region based on the Brunt-Vaisala frequency calculations as mentioned in the methodology. The spatiotemporal variability of Vaisala frequency is displayed in the contours in Figure 11(a and b) for the upper mesosphere region (90 and 85 km) and in Figure 11(c and d) for the lower mesosphere region (75 and 70 km). Based on N^2, the upper inversion instability is maximum at 90 km (~0.027) and at 85 km (~0.029) relative to the lower inversion instability at 75 km (~0.033) and 70 km (~0.035). This result leads us to the conclusion that a high amount of gravity wave potential energy is a consequence of the high instability of the upper inversion relative to the lower.

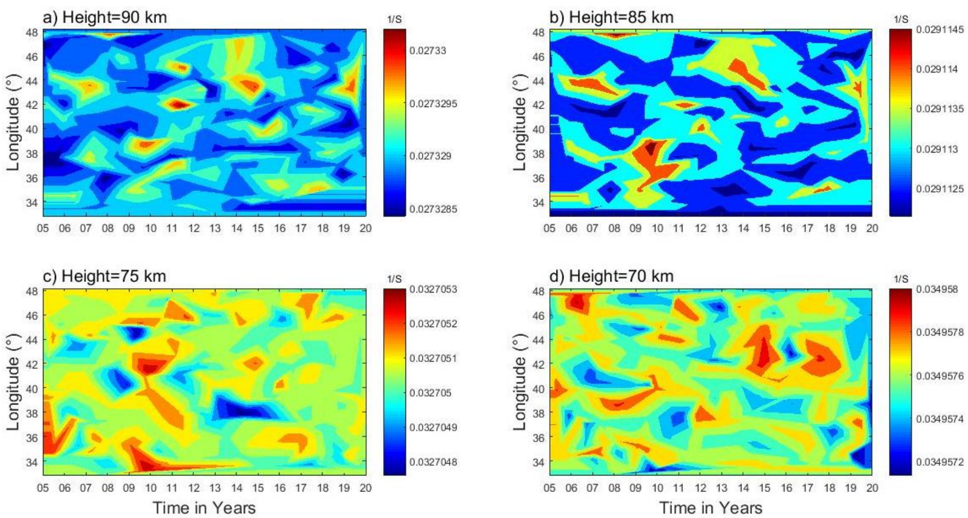

Figure 11. Brunt-Vaisala frequency (N^2) profiles for the upper (85 and 90 km) and lower (70 and 75 km) mesosphere regions.

4. Conclusions

In this article, 16 years of SABER mesosphere temperature profiles are utilized to investigate the MIL phenomenon and its causative mechanism through gravity wave potential energy (P_E) and instability criteria of Bruent-Vaisala frequency (N^2) over low latitude bands (3-15^0 N). The observational conclusions from this chapter are drawn as follows:

https://doi.org/10.5194/angeo-2023-34
Preprint. Discussion started: 30 November 2023

Annales Geophysicae Discussions
Open Access

- ✓ The frequency of occurrence in the upper and lower mesosphere regions reveals that the mean occurrence rate for upper mesosphere inversions lies below 40% and for lower inversions below 20%.
- ✓ Based on the analysis of frequency of occurrence on mesospheric inversion layer (MIL) characteristic features, it is revealed that the most probable value for upper inversion amplitude is 38 k with standard deviations (SD) of 1.72 k, inversion layer thicknesses are 5.5 km with SD of 2.3 km, and the base height is 78 km with an SD of 2.8 km. Whereas the lower inversion amplitude is 25 K with an SD of 14.5 K, the inversion layer thickness is 3.8 km with SD of 1.72 km and a base height of 73 km with an SD of 2.07 km.
- ✓ The gravity wave indicator potential energy depicts high energy (below 100 J/kg) at the upper mesosphere region (85 and 90 km) compared to the lower mesosphere region (75 and 70 km) with less than 50 J/kg.
- ✓ The stability criteria at the mesosphere region are indicated by Brunt-Vaisala frequency (N^2), which shows low values at the upper mesosphere region (90 and 85 km) relative to the lower mesosphere region (75 and 70 km), leading to the conclusion that the high potential energy at the upper mesosphere region is due to the instability over that region, which gives rise to large inversion phenomena.
- ✓ In general, we concluded that the processes in the atmosphere vary from region to region. As a result, the atmospheric state varies significantly with altitude as well as from place to place and time to time.

Data availability. The SABER data are freely available via the link at http://saber.gats-inc.com/index.php.

Author contribution. Chalachew Lingerew: data curation, investigation, software, visualization, writing the original draft, and writing review. U. Jaya Prakash Raju; supervision, and editing.

Competing interest. The authors declare that they have no conflict of interest relevant to this study.

Acknowledgments. The Authors would like to express their gratitude to the National Aeronautics and Space Administration (NASA) for providing the SABER data downloaded from the website: http://saber.gats-inc.com/index.php.

https://doi.org/10.5194/angeo-2023-34
Preprint. Discussion started: 30 November 2023

Annales Geophysicae Discussions Open Access

References

Bizuneh, C.L., Prakash, R., and Nigussie, M.: Long-term temperature and ozone response to natural drivers in the mesospheric region using 16 years (2005–2020) of TIMED/SABER observation data at 5-15^{0}N. Advances in Space Research, 70, 2095–2111, https://doi.org/10.1016/j.asr.2022.06.051, 2022.

Collins, R. L., Lehmacher, G. A., Larsen, M. F., and Mizutani, K.: Estimates of vertical eddy diffusivity in the upper mesosphere in the presence of a mesospheric inversion layer, Ann. Geophys., 29(11), 2019–2029, http://doi:10.5194/angeo-29-2019-2011, 2011.

Cutler, L. J., Collins, R. L., Mizutani, K., and Itabe, T.: Rayleigh lidar observations of mesospheric inversion layers at Poker Flat, Alaska (65^0 N, 14^0 W), Geophys. Res. Lett., 28, 1467–1470, https://doi.org/10.1029/2000GL012535, 2001.

Duck, T. J., Sipler, D. P., and Salah, J. E.: Rayleigh lidar observations of a mesospheric inversion layer during night and day, Geophys. Res. Lett., 28, 3597–3600, 2001.

Duck, T. J. and Greene, M. D.: High Arctic observations of mesospheric inversion layers, Geophys. Res. Lett., 31, L02105, https://doi.org/10.1029/2003GL018481, 2004.

Eckermann, S.D., Hirota, I., and Hocking, W. K.: Gravity wave and equatorial wave morphology of the stratosphere derived from long-term rocket soundings. Q. J. R. Meteorol. Soc., 121, 149 186, http://doi.org/10.1002/qj.49712152108, 1994.

Emanuel, K.A.: Atmospheric Convection, Oxford University Press, New York, 580pp, 1994.

Fechine, J., Wrasse, C. M., Takahashi, H., Mlynczak, M. G., and Russell, J. M.: Lower-mesospheric inversion layers over Brazilian equatorial region using TIMED/SABER temperature profiles, Adv. Space Res., 41, 1447–1453, https://doi.org/10.1016/j.asr.2007.04.070, 2008.

Fritts, D. C., Wang, L., Laughman, B., Lund, T. S., & Collins, R. L.: Gravity wave dynamics in a mesospheric inversion layer: 2. Instabilities, turbulence, fluxes, and mixing. Journal of Geophysical Research: Atmospheres, 123, 649–670, https://doi.org/10.1002/2017JD027442, 2018.

Fritts, D. C., and Alexander, M. J.: Gravity wave dynamics and effects in the middle atmosphere, Rev. Geophys., 41, 1003, https://doi.org/10.1029/2001RG000106, 2003.

Fritts, D. C., Laughman, B., Wang, L., Lund, T. S., & Collins, R. L.: Gravity wave dynamics in a mesospheric inversion layer: 1. Reflection, trapping, and instability dynamics. Journal of Geophysical Research: Atmospheres, 123, 626-648, https://doi.org/10.1002/2017JD027440, 2018.

https://doi.org/10.5194/angeo-2023-34
Preprint. Discussion started: 30 November 2023

Annales Geophysicae Discussions

Gan, Q., Zhang, S. D., and Yi, F.: TIMED/SABER observations of lower mesospheric inversion layers at low and middle latitudes, J. Geophys. Res., 117, D07109, https://doi:0.1029/2012JD017455, 2012.

Hirota, I.: Climatology of gravity waves in the middle atmosphere. J. Atmos. Terr. Phys., 46, 767–773, http://doi.org/10.2151/jmsj1965.63.6-1055, 1984.

Hamilton, K.: Climatological Statistics of Stratospheric Inertia-Gravity Waves Deduced from Historical Rocket-sonde Wind and Temperature Data. J. Geophys. Res., 96, 20831–20839, http://doi.org/10.1029/91JD02188, 1991.

Holton, J. R.: The influence of gravity wave breaking on the general circulation of the middle atmosphere, J. Atmos. Sci., 40, 2497–2507, 1983.

Irving, B. K., Collins, R. L., Lieberman, R. S., Thurairajah, B., and Mizutani, K.: Mesospheric Inversion Layers at Chatanika, Alaska (65°N, 147°W): Rayleigh lidar observations and analysis, J. Geophys. Res. Atmos., 119, 11,235–249, http://doi:10.1002/2014JD021838, 2014.

John, S.R., Kumar, K. K.: TIMED/SABER observations of global gravity wave climatology and their interannual variability from stratosphere to mesosphere lower thermosphere. Clim. Dyn., 39, 1489–1505, http://doi.org/10.1007/s00382-012-1329-9, 2012.

Leblanc, T., McDermid, I. S., Hauchecorne, A., and Keck hut, P.: Evaluation of optimization of lidar temperature analysis algorithms using simulated data, J. Geophys. Res., 103, 6177–6187, 1998.

Leblanc, T., and Hauchecorne, A.: Recent observations of mesospheric temperature inversions, J. Geophys. Res., 102, 19471–19482, https://doi.org/10.1029/97JD01445, 1997.

Lindzen, R. S.: Turbulence and stress due to gravity waves and tidal breakdown, J. Geophys. Res., 86, 9707–9714, https://doi:10.1029/JC086iC10p09707, 1981.

Lingerew, C., Jaya Prakash Raju, U., & Guimarães Santos, C. A.: NN-MLT model prediction for low-latitude region based on artificial neural network and long-term SABER observations. *Earth and Space Science*, *10*, e2023EA002930, https://doi.org/10.1029/2023 EA002930, 2023.

Mlynczak, M. G., Marshall, B. T., Martin-Torres, F. J., Russell III, J. M., Thompson, R. E., Remsberg, E. E., and Gordley, L. L.: Sounding of the Atmosphere using Broadband Emission Radiometry observations of daytime mesospheric O_2 (1Δ) 1.27 μm emission and derivation of ozone, atomic oxygen, and solar and chemical energy deposition rates, 2007.

Meriwether, J. W., and Gerrard, A. J.: Mesosphere inversion layers and stratosphere temperature enhancements, Rev. Geophys., 42, RG3003, http//doi:10.1029/2003RG000133, 2004.

Meriwether, J. W., and Gardner, C. S.: A review of the mesosphere inversion layer phenomenon, J. Geophys. Res., 105, 12 405–12 416, 2000.

Nath, O., & Sridharan, S.: Long-term variabilities and tendencies in zonal mean TIMED–SABER ozone and temperature in the middle atmosphere at 10–15°N. Journal of Atmospheric and Solar-Terrestrial Physics, 120, 1–8, https://doi:10.1016/j.jastp.2014.08.010, 2014.

Ramesh, K., Sridharan, S.: Large mesospheric inversion layer due to breaking of small scale gravity waves: Evidence from Rayleigh lidar observations over Gadanki (13.51^0 N, 79.21^0 E). J. Atmos. Sol. Terr. Phys. 89, 90–97, http://doi.org/10.1016/j.jastp.2012.08.011, 2012.

Ramesh, K., Sridharan, S. and Vijaya Bhaskara, S.: Causative mechanisms for the occurrence of a triple layered mesospheric inversion event over low latitudes, J. Geophys. Res. Space Physics, 119, 3930–3943, http://doi:10.1002/2013JA019750, 2014.

Ramesh, K., Sridharan, S., Raghunath, K., and Rao, S. V. B.: A chemical perspective of day and night tropical (10°N–15°N) mesospheric inversion layers, J. Geophys. Res. Space Physics, 122, http://doi:10.1002/2016JA023721, 2017.

Ramesh, K., Sridharan, S., Vijaya Bhaskara Rao, S., Raghunth, K., Bhavani Kumar, K.: Rayleigh lidar observations of mesospheric inversion layers over Gadanki (13.5^0N, 79.2^0 E) and their relation with gravity wave activities. Indian Journal of Radio and space science, 43, 83-90, 2013.

Remsberg, E., Lingenfelser,V., Harvey,V., Grose, W., Russell III, J., Mlynczak, M., Gordley, L., and Marshall, B. T.: The verification of the quality of SABER temperature, geopotential height, and wind fields by comparison with Met Office assimilated analyses, J. Geophys. Res., 108(D19), 4628, https://doi:10.1029/2003JD003720, 2003.

Russell, J.M., Mlynczak, M.G., Gordley, L.L., Tansock, J., Esplin, R.: An overview of the SABER experiment and preliminary calibration results. In Proceedings of the SPIE, 44th Annual Meeting, Denver, CO, USA, 3756, 277–288, 1999.

Sica, R. J., Argall, P. S., Shepherd, T. G., and Koshyk, J. N.: Model-measurement comparison of mesospheric temperature inversions, and a simple theory for their occurrence, Geophys. Res. Lett., 34, L23806, https://doi:10.1029/2007GL030627, 2007.

Siva Kumar, V., Bhavani Kumar, Y., Raghunath, K., Rao, P. B., Krishnaiah, M., Mizutani, K., Aoki, T., Yasui, M., and Itabe, T.: Lidar measurements of mesospheric temperature inversion at a low latitude, Ann. Geophys., 19, 1039–1044, https://doi.org/10.5194/angeo-19-1039-2001, 2001.

https://doi.org/10.5194/angeo-2023-34
Preprint. Discussion started: 30 November 2023

Sridharan, S., Sathishkumar, S., and Gurubaran, S.: Influence of gravity waves and tides on mesospheric temperature inversion layers: simultaneous Rayleigh lidar and MF radar observations, Ann. Geophys., 26, 3731–3739, 2008.

Singh, R. P., & Pallamraju, D.: Mesospheric temperature inversions observed in OH and O2 rotational temperatures from Mount Abu (24.6°N, 72.8°E), India. Journal of Geophysical Research: Space Physics, 123, 8823–8834, https://doi.org/10.1029/2018JA025703, 2018.

Smith, A.: Global Dynamics of the MLT, Surv. Geophys., 33, 1177–1230, https://doi.org/10.1007/s10712-012-9196-9, 2012.

Szewczyk, A., Strelnikov, B., Rapp, M., Strelnikova, I., Baumgarten, G., Kaifler, N., Dunker, T., and Hoppe, U. P.: Simultaneous observations of a Mesospheric Inversion Layer and turbulence during the ECOMA-2010 rocket campaign, Ann. Geophys., 31, 775–785, http://doi:10.5194/angeo-31-775-2013, 2013.

Wang, L., Geller, M.A., Alexander, M.J.: Spatial and Temporal Variations of Gravity Wave Parameters. Part I: Intrinsic Frequency, Wavelength, and Vertical Propagation Direction. J. Atmos. Sci., 62, 125–142, http://doi.org/10.1029/2010JD013860, 2005.

Wang, L., and Alexander, M.J.: Global estimates of gravity wave parameters from GPS radio occultation temperature data. J. Geophys.Res. 115, D21122, http://doi.org/10.1029/2010JD013860, 2010.

Walterscheid, R. L., and Hickey, M. P.: Gravity wave ducting in the upper mesosphere and lower thermosphere duct system, J. Geophys. Res., 114, D19109, http://doi:10.1029/2008JD 011269, 2009.

Yuan, T., Pautet, P. D., Zhao, Y., Cai, X., Criddle, N. R., Taylor, M. J., and Pendleton, W. R.: Coordinated investigation of mid-latitude upper mesospheric temperature inversion layers and the associated gravity wave forcing in Logan, Utah, J. Geophys. Res. Atmos., 119, 3756–3769, http://doi:10.1002/2013JD020586, 2014.